Time resolved photoelectron spectroscopy of iodide-4-thiouracil cluster: the $\pi\pi^*$ state as a doorway for electron attachment

Megan Asplund, [1] *Masafumi Koga,*[1]*, Ying Jung Wu,*[1] *and Daniel M Neumark*[1,2] *

[1]*Department of Chemistry, University of California, Berkeley, California 94720, USA*

[2]*Chemical Sciences Division, Lawrence Berkeley National Laboratory, Berkeley, California 94720, USA*

Abstract

The photophysics of thiobases — nucleobases in which one or more oxygen atoms are replaced with sulfur atoms — have been shown to vary greatly depending on the location of sulfonation. Not only are direct dynamics of the neutral thiobase impacted, but also the dynamics of excess electron accommodation. In this work, time resolved photoelectron spectroscopy (TRPES) is used to measure binary anionic clusters of iodide and 4-thiouracil, I^-·4TU. We investigate charge transfer dynamics driven by excitation at 3.88 eV, corresponding to the lowest $\pi\pi^*$ transition of the thiouracil, and at 4.16 eV, near the cluster vertical detachment energy. The photoexcited state dynamics are probed by photodetachment with 1.55 eV and 3.14 eV pulses. Excitation at 3.88 eV leads to signal from a valence-bound ion only, indicating a charge accommodation mechanism that does not involve a dipole-bound anion as an intermediate. Excitation at 4.16 eV rapidly gives rise to dipole-bound and valence-bound ion signals, with a second rise in valence-bound signal corresponding to the decay of the dipole-bound signal. The dynamics associated with the low energy $\pi\pi^*$ excitation of 4-thiouracil provide clear experimental proof for the importance of localized excitation and electron backfilling in halide-nucleobase clusters.

I. Introduction

The photophysics of natural nucleobases have been studied extensively owing to their biological significance and the role that fast non-adiabatic relaxation plays in their high photostability.[1-8] In contrast, single atom substitutions, such as the replacement of one or both nucleobase oxygens with sulfur atoms, have been shown to have profound impacts on relaxation pathways following photoexcitation.[9-17] These nucleobase derivatives are of interest owing to their potential for pharmacological applications such as phototherapy where they can act as photosensitizers.[9-11, 18, 19] For example, upon photoexcitation of sulfur substituted nucleobases, the quantum yield for relaxation to the triplet manifold nears unity, resulting in increased reactivity compared to canonical nucleobases that undergo rapid relaxation to their ground electronic states.[7, 9, 11, 14, 17] It is also of interest to contrast the interactions of natural and thio-substituted nucleobases with low energy electrons, since this interaction is also important in radiation chemistry and biology. This latter consideration motivates the present study, which examines the dynamics of photoexcited I^-·4-thiouracil (I^-·4TU) cluster anions and builds on our previous work on I^-·2-thiouracil (I^-·2TU) to elucidate the effects of sulfonation on charge transfer mechanisms.

Within a cell, DNA damage may occur via direct or indirect interactions between photons and a DNA strand. In particular, indirect interactions via low energy electrons have been implicated as a significant contributor to strand breakages.[20, 21] These considerations have motivated electron scattering and photoionization studies of gas phase canonical and modified nucleobase species,[22] as the nucleobase is predicted to be the initial site of electron attachment.[23-26] Dissociative electron attachment (DEA) measurements show that the major product of interactions of nucleobases and low energy (<3 eV) electrons is H loss from the base via NH bond ruptures.[27-31] DEA studies of 2-thiouracil (2TU) similarly show that NH bond cleavage accounts for the majority of dissociation

products,[32-34] though equivalent results have not been published for 4-thiouracil.

Electron scattering experiments are complemented by photoelectron spectroscopy (PES) of nucleobase anions. These experiments demonstrate that during electron capture, a low energy electron may become associated with a nucleobase as either a dipole-bound (DB) or valence-bound (VB) anion, which are readily distinguished by their spectroscopic signals.[35-37] DB anions can only form for a molecule with a sufficiently large dipole moment,[38, 39] as they are the result of association between an excess electron and a molecular dipole. DB anions are generally weakly bound, with a geometry relatively unperturbed relative to the neutral. An excess electron can also be captured by one of the unoccupied valence (usually anti-bonding) orbitals of the molecule, forming a VB anion. In nucleobases, the VB anion forms by population of the π^* orbital, causing a ring puckering distortion of the molecule.[40, 41] PES of uracil anions shows features from both DB and VB anions, with an intense, sharp feature at low binding energy, corresponding to a DB anion, as well as a broader feature associated with a rare tautomer valence anion.[35, 36]

Photoelectron spectroscopy of the 4-thiouracil and dithiouracil anions by Bowen and co-workers,[42] supported by computational work,[43] demonstrates that both thiobases can form stable valence-bound anions in their canonical forms. These data show no evidence for stable dipole-bound anions for either thiobase. However, DEA of 2TU implicates a DB state in facilitating dissociative electron attachment to the thiobase,[32] indicating the possible importance of transient DB anions in these systems.

The dynamics of electron capture have been investigated for several nucleobases by time-resolved photoelectron spectroscopy (TRPES)[41] and one-photon photodepletion spectroscopy of iodide-nucleobase clusters.[44] In TRPES experiments, the halide anion acts as an electron donor, with charge transfer instigated by a femtosecond UV pump pulse. The resultant transient negative

ions of the nucleobase are probed by a second femtosecond laser pulse that detaches the excess electron. We have previously carried out experiments on iodide-nucleobase clusters, including iodide-uracil,[45-47] iodide-thymine,[47, 48] iodide-adenine,[49] iodide-uracil H_2O,[50, 51] and iodide-2-thiouracil[52], while photodepletion measurement have been applied to clusters of iodide with all of the canonical DNA and RNA nucleobases,[44, 46, 53] as well as iodide-2-thiouracil, iodide-4-thiouracil, and iodide-2,4-thiouracil.[54, 55]

In each of the systems measured by TRPES, the DB anion is formed when the cluster is excited near its vertical detachment energy (VDE, near 4 eV for these clusters), exciting the excess electron into a DB state of the complex. One also observes rapid formation of VB states upon near-VDE excitation, although direct excitation of an electron into the VB state is not generally favorable. In measurements where the cluster is excited near its VDE, DB signal arises more quickly than VB signal, suggesting that the DB state acts as a gateway state. However, VB signal is also observed in experiments with higher energy excitation (4.7 eV), wherein there is no evidence of DB ion formation. Although we originally proposed that photoexcitation directly transferred an electron from the I^- into a VB state of the nucleobase, subsequent work suggested an alternate mechanism in which the UV pump pulse excites the strong $\pi\pi^*$ absorption of the

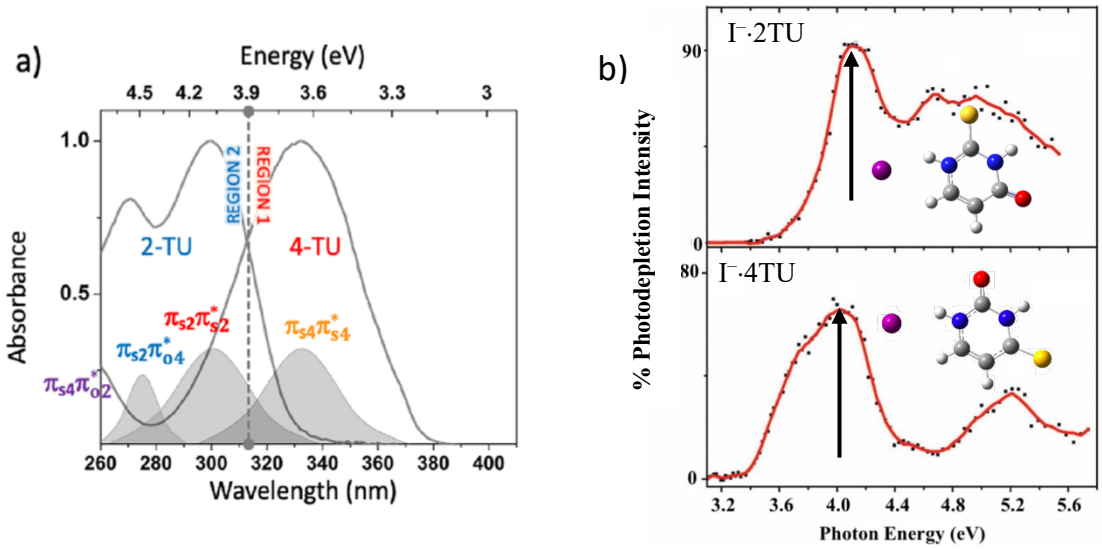

Figure 1: a)Absorption spectra of 2TU and 4TU in carbon tetrachloride solution with bands assigned to specific $\pi\pi^*$ transitions adapted from Mohamadzade et al[10] b) Gas phase photodepletion spectra of I^-·2TU and I^-·4TU adapted from Uleanya et al[42] with optimized geometries for both clusters and arrows representing the VDE of each cluster.

nucleobase followed by electron transfer from the I^- into the π vacancy.[46] Thus far, however, direct experimental evidence for either mechanism has been elusive.

The cluster I^-·4TU offers an opportunity to examine how VB chromophore ions can form without the involvement of a DB state. As shown in Fig. 1, the isolated thiobase 4TU has a particularly low energy $\pi\pi^*$ excitation relative to other nucleobases such as uracil or 2TU,[17] and photodepletion measurements of the I^-·4TU cluster[55] show an electronic absorbance below the VDE of the cluster (Fig. 1, right panel). This presents an opportunity to isolate the potential impact of $\pi\pi^*$ excitation while minimizing the contributions of higher energy electron scattering mechanisms. Additionally, as I^-·4TU DB anions are easily distinguished from localized excitations by TRPES, a short-lived DB anion signal for the cluster can in principle be separated from the broad shoulder at ~3.8 eV observed by photodepletion spectroscopy.

In this study, we use TRPES of the iodide-4-thiouracil cluster to investigate its dynamics

following excitation of a $\pi\pi^*$ transition below the cluster VDE, as well as higher energy excitation near the cluster VDE. Our results at the lower excitation energy isolate dynamics following $\pi\pi^*$ excitation, providing empirical evidence for the VB formation mechanism previously postulated wherein $\pi\pi^*$ chromophore localized excitation allows the excess electron to occupy a π orbital vacancy. This mechanism can proceed without a DB anion intermediate. At excitation near the cluster VDE, we confirm the existence of a transient DB state and characterize formation of the VB anion with two rise times, with the first caused by chromophore excitation and the second by DB anion to VB anion conversion.

II. Methods

The TRPES setup has been described in other publications,[56, 57] but a brief summary will be provided here. An inert carrier gas, in this case argon, flows over a reservoir of methyl iodide and through a cartridge containing the solid 4-thiouracil sample (97%, Alfa Aesar). An Even-Lavie pulsed valve heated to 220° C and operating at 500 Hz generates a gas pulse that passes through an ionizing filament. Iodide anions are produced from dissociative electron attachment to CH_3I, which then cluster to gas phase 4-thiouracil to make the species of interest. Ions in the pulsed beam are extracted perpendicularly by a Wiley McLaren time-of-flight mass spectrometer[58] that includes a mass gate to selectively pass iodide-4-thiouracil clusters.

In the interaction region, pump and probe laser pulses intersect with the cluster packets within a velocity-map imaging assembly. The photodetached electrons are detected by a pair of chevron-stacked microchannel plates coupled to a phosphor screen. The phosphor screen is read by a CCD camera, and the raw data images are processed using BASEX[59] to generate the kinetic energy spectra and angular distributions of the photoelectrons.

Laser pulses are generated by KM Griffin Oscillator and KM Dragon Amplifier, producing ~2 mJ/pulse at 1000 Hz repetition rate, with the fundamental centered at 1.55 eV and a pulse duration of approximately 35 fs. To generate the pump pulse, a portion of this output is directed into a TOPAS-C optical parametric amplifier to generate tunable visible light, which is subsequently doubled by a BBO crystal to obtain the final UV excitation wavelength. The remainder of the laser pulse serves as the probe (detachment) pulse. It can be directed into a delay stage and used to trace the time evolution of transient anion species of the chromophore. Alternatively, it can be frequency doubled by a BBO and the subsequent 3.14 eV probe pulse can photodetach free atomic I^-, one of the major dissociation products for the cluster. The cross-correlation of the pump and probe pulses sets the instrumental response time at about 80fs.

Dissociation of the I^-·4TU cluster to I^- and 4TU was investigated theoretically using the Gaussian 16 computing package[60] at the MP2 level of theory with an augmented Dunning basis set aug-cc-pVDZ for C, H, O, and N, and an additional set of diffuse functions (aug-cc-pVDZ-pp) for I.[61]

III. Results

Figure 2 shows one color photoelectron spectra collected at hυ=3.88 eV and 4.92 eV, just under and well above the expected cluster VDE of 4 eV based on photodepletion spectroscopy.[55] The most intense feature of the spectrum at 4.92 eV excitation is a peak centered at an electron kinetic energy (eKE) of 0.74 eV, or a binding energy of 4.18 eV, with binding energy defined as eBE= hυ-eKE. Based on previous work on related systems,[41] this feature is assigned to direct detachment to the I($^2P_{3/2}$) ·4TU spin-orbit state of the neutral cluster and VDE=4.18 eV for I^-·4TU. This value is close to the calculated VDE from Uleanya et al (4.32eV),[55] as well as the VDE values for iodide-thymine, iodide-uracil, and iodide-thiouracil clusters.[41, 45, 47, 48, 52] A second, less intense feature is seen near 0 eKE and corresponds to resonant excitation of the cluster followed by electron autodetachment, as previously determined for similar clusters.[47, 48, 51]

The spectrum collected at 3.88 eV excitation has a single feature at low eKE. This excitation is below the VDE of the cluster, so the signal is due to autodetachment or direct detachment below the VDE.

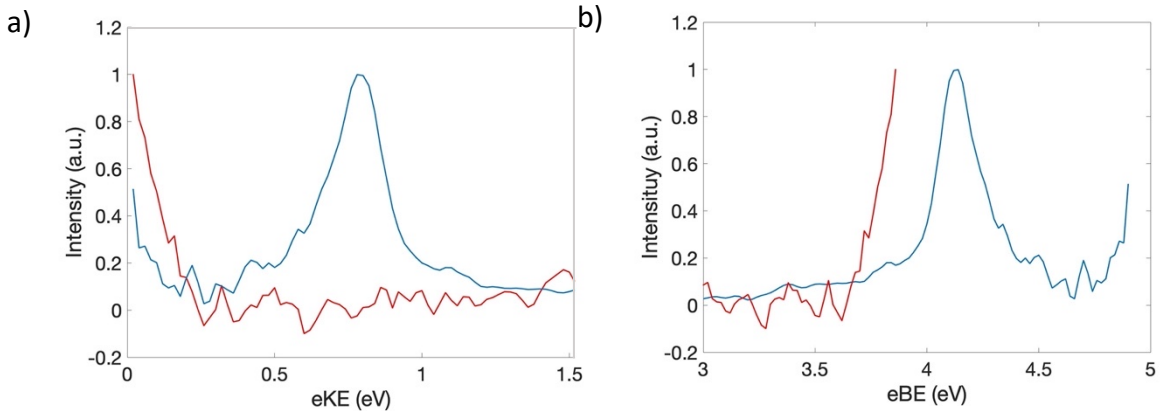

Figure 2. One color spectra of I^-·4TU collected with 4.92eV (blue) and 3.88eV (red) excitation plotted in electron kinetic energy (a) and electron binding energy (b)

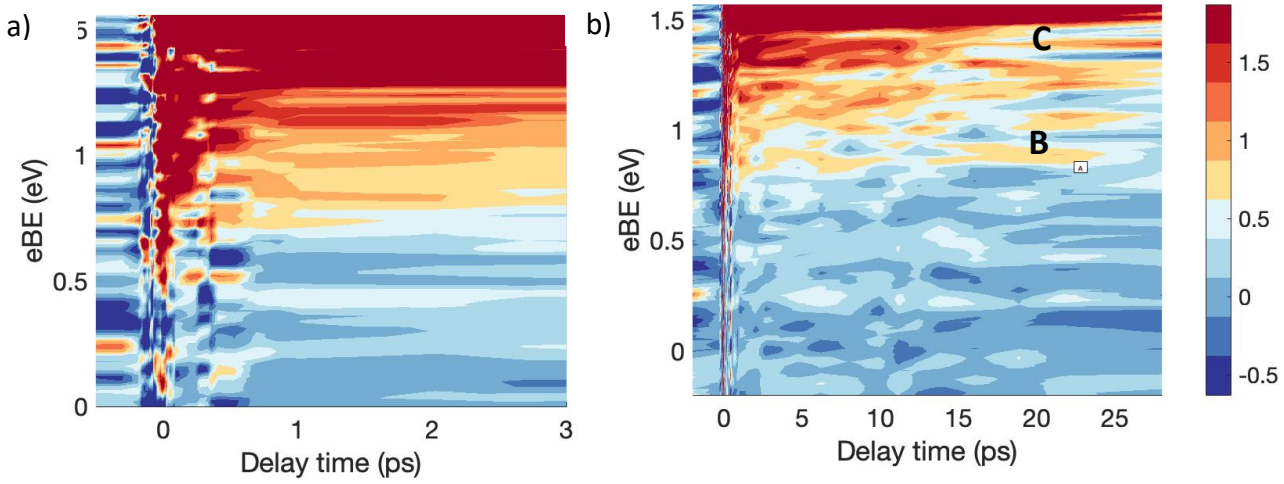

Figure 3. Contour plot of I^{-}·4TU TRPE spectra with 3.88eV pump and 1.55eV probe pulses at shorter (panel a) and longer (panel b) delay times.

Figure 3 shows contour plots of time-resolved photoelectron spectra at shorter (a) and longer (b) pump-probe delays at a pump photon energy of 3.88 eV, corresponding to the low energy $\pi\pi^*$ excitation of the chromophore, and a 1.55 eV probe pulse. There are two primary features apparent in Fig. 3. The first, labeled feature C in the right panel, is very intense and occurs mainly between 1.5 and 1.55 eBE, corresponding to near-zero (0-0.05 eV) kinetic energies. This is the energy range expected for autodetachment and it appears that this signal is enhanced at positive pump-probe delays. The spectra also show a broad feature B from 0.8 to 1.4 eV, which corresponds well with the VDE of the 4TU valence-bound ion as measured by one photon photoelectron spectroscopy by Li et al (0.7–1.5 eV).[42] The feature arises very quickly after t_0 before losing most of its intensity within a few hundred femtoseconds.

Figure 4 shows the analogous contour plots of TRPES measurements taken with 4.16 eV (near VDE) excitation and 1.55 eV probe and exhibits three distinct features. Near t_0, two of these features look quite similar to features B and C in Figure 3 and are labeled accordingly. Notably, feature B is much longer lived in these spectra than the spectra with 3.88eV excitation. The third

feature in Figure 4, feature A, is distinct from any feature in Figure 3. It covers 0-0.3eV, and has a much narrower spectral profile than feature B. In previous measurements of iodide-chromophore clusters, features similar to feature A have been ubiquitous in near VDE excitation measurements.[41, 46, 49-51, 62] Based on its narrow shape and low binding energy, feature A can be labeled as signal from a transient dipole-bound anion.

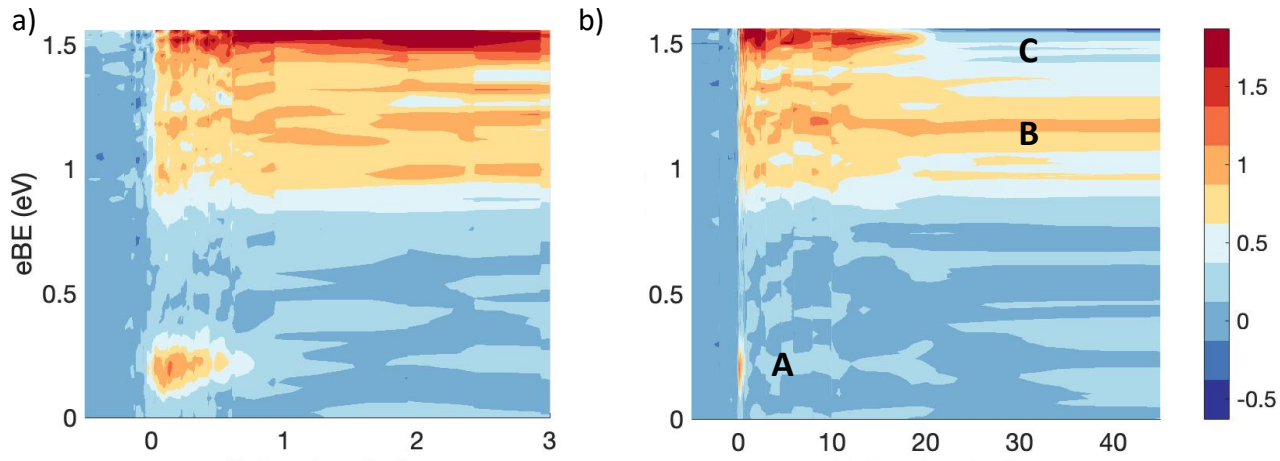

Figure 4. Contour plot of I^-·4TU TRPE spectra with 4.16 eV pump and 1.55 eV probe pulses at shorter (panel a) and longer (panel b) delay times

Dynamics at both excitation energies were also probed at 3.14 eV. This energy is sufficient to just detach bare I^- to neutral iodine. Figure 5 shows the contour plots of measurements with a 3.14 eV probe pulse and 3.88 eV (a) or 4.16 eV (b) pump pulses. The spectra are dominated by a single feature (D) at eBE=3.06 eV, the electron affinity of atomic iodine.[63] Feature D corresponds to photodetachment of the iodide fragment following dissociation of the photoexcited cluster to I^- + 4TU and has been seen in our previous studies of iodide-nucleobase complexes.[41, 46, 50, 64]

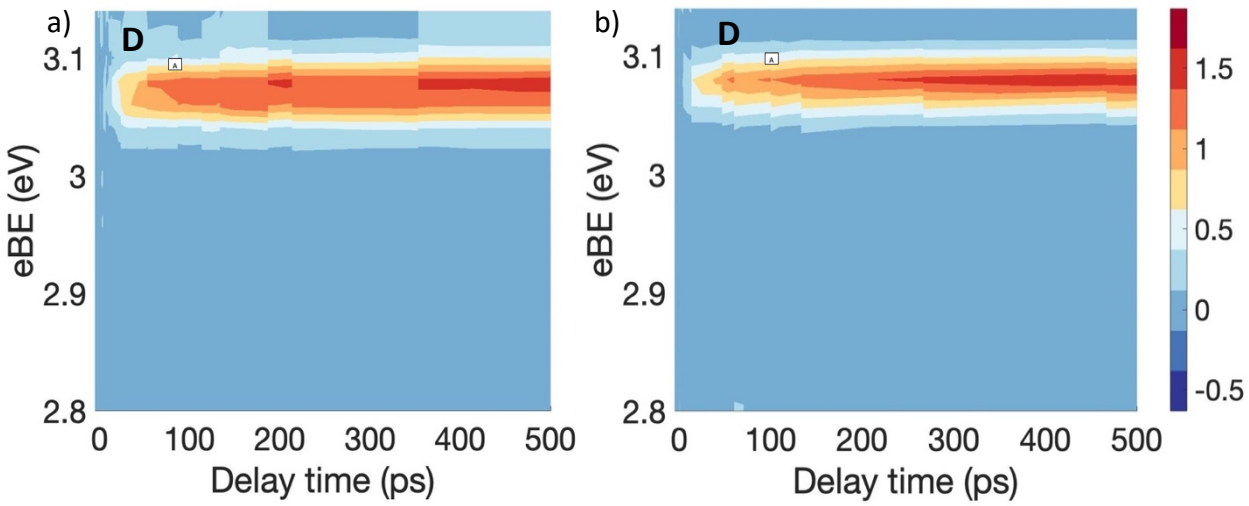

Figure 5. Contour plot of I^-4TU TRPE spectra with 3.88eV (panel a) and 4.16 eV (panel (b) pump and 3.14 eV probe pulses

IV. Analysis

The dynamics of this system are analyzed by integrating over features of the acquired spectra and then fitting the integrations to a convolution of a Gaussian experimental response function and a sum of exponential functions (Eq 1).

$$I(t) = \frac{1}{\sigma_{CC}\sqrt{2\pi}} \exp\left(-\frac{t^2}{2\sigma_{CC}^2}\right) \cdot \begin{cases} I_0\,, & t < 0 \\ I_0 + \sum_i A_i \exp\left(\frac{-t}{\tau_i}\right) + c\,, & t \geq 0 \end{cases} \quad (1)$$

In this equation, I_0 is a constant offset from background signal, σ_{CC} is the experimental response time of 80 fs, c is the signal offset at very long time delays, and A_i and τ_i are the intensity and time constant for the ith exponential function. The time evolution for several of these signals is complex, requiring multiple exponential terms to adequately fit the integrated plot. The integrated normalized intensities of features from the spectra collected with 3.88 eV excitation and 1.55 eV probe are plotted in Fig 6 with the corresponding parameters for Eq. 1 reported in Table 1. Integrated normalized intensities of features collected with 4.16 eV excitation and 1.55 eV probe are plotted in Fig 7 with fitting parameters reported in Table 2. In Fig 6 and 7, data are indicated by open circles and the fits by solid lines.

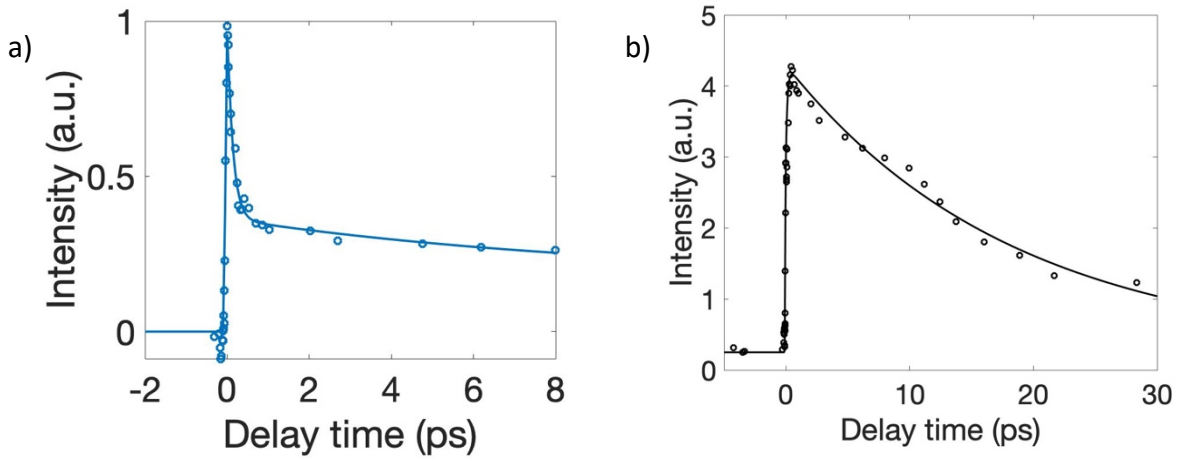

Figure 6. Time evolution of integrated features B (blue, VB, panel a) and C (black, AD, panel b) for 3.88eV excitation, 1.55eV probe . Signals are scaled from raw data to normalize the maximum intensity of feature B to 1.

Table 1. Fit parameters that reproduce the time evolution in Fig. 6.

	eBE (eV)	τ_1 decay (fs)	τ_2 rise (fs)	τ_3 decay (ps)	A_1	A_2	A_3	c
Feature C	1.50 – 1.55		218 ± 93	18.4 ± 2.3		-0.51	1.0	
Feature B	0.7 – 1.2	139 ± 36		9.4 ± 4.7	0.81[a]		0.19	0.17

[a] All amplitudes shown here are normalized by the sum of the exponential amplitudes.

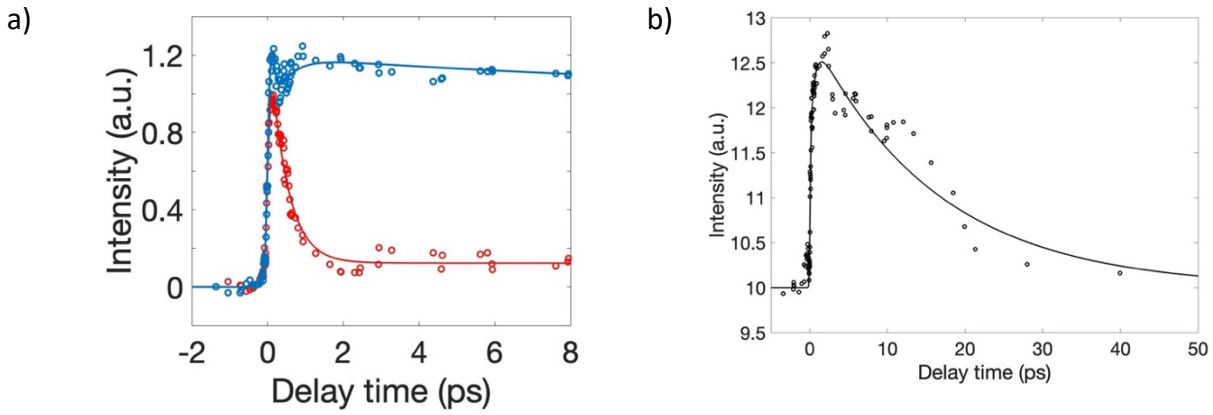

Figure 7. Time evolution of integrated feature A (red, DB), feature B signal (blue, VB) signal, and feature C (black, AD) for 4.16eV excitation, 1.55eV probe spectra. Feature A and B are normalized to maximum values of 1 and 1.2 respectively (panel a). Feature C is scaled using the normalization factors for feature A (panel b).

Table 2. Fit parameters that reproduce the time evolution in Fig 7.

	eBE (eV)	τ_1 (fs) decay	τ_2 (fs) rise	τ_3 (ps) decay	A_1	A_2	A_3	c
Feature C	1.50 – 1.55		560 ± 390	16.2 ± 3.8		-0.51	1.0	
Feature B	0.7 – 1.2	47.4 ± 6.3	442[b]	13.1 ± 9.9	0.96[a]	-0.07	0.04	0.83
Feature A	0 – 0.30	442 ± 50						

[a] All amplitudes shown here are normalized by the sum of the decay amplitudes.
[b] Value fixed using decay of DB signal

In Fig. 6a, signal from feature B rises within the experimental resolution of 80 fs and decays biexponentially, with 80% of the signal decaying in τ_1=140 fs and an additional fraction decaying with τ_2=9.4 ps. At later times, the signal reaches an asymptotic value with a significant offset. The signal from feature C rises within about τ_2=200 fs and then exhibits single exponential decay with τ_3=18.4 ps.

Figure 7 shows the temporal evolution of the three features seen in Fig. 4. In Fig. 7a, feature A (red, DB anion) rises within the experimental resolution before undergoing single exponential decay with τ_1=440fs. A small signal offset remains at long time delays attributed to background

noise. The signal from feature B (blue, VB anion) requires three time constants to fit accurately. The signal rises within instrument resolution, decays partially (with time constant τ_1), undergoes a second rise (τ_2), then decays slowly (τ_3) before reaching an asymptotic offset. Qualitative examination of Fig 7, as well as known mechanisms for DB state mediated VB ion formation,[30, 45, 52, 65, 66] suggests that depletion of the DB ion gives rise to the VB ion as the former state transitions into the latter. Accordingly, the rise τ_2 for the VB signal should be roughly equal to decay τ_1 for the DB signal. With three variable time constants, the precision of the fit is unacceptably low. If we fix τ_2 for the VB signal to 440 fs, i.e. τ_1 for feature A, we retrieve 47 fs for the initial VB decay constant τ_1. The signal continues to decay with τ_3 = 13.1 ps.

Feature C in Fig. 7b has a rise time of τ_2=560 fs and decays with τ_3=16.2 ps. The fit for the AD signal is not as good as for the DB and VB signal, likely because of the narrow energy window for the integration, which is selected to minimize overlap with the VB feature.

The VDE of the DB ion shifts noticeably over the first picosecond following excitation. This can be better quantified by fitting feature C to a Gaussian function at each delay time and plotting the binding energy of the Gaussian peak over time, as shown in Figure 8. Because of the

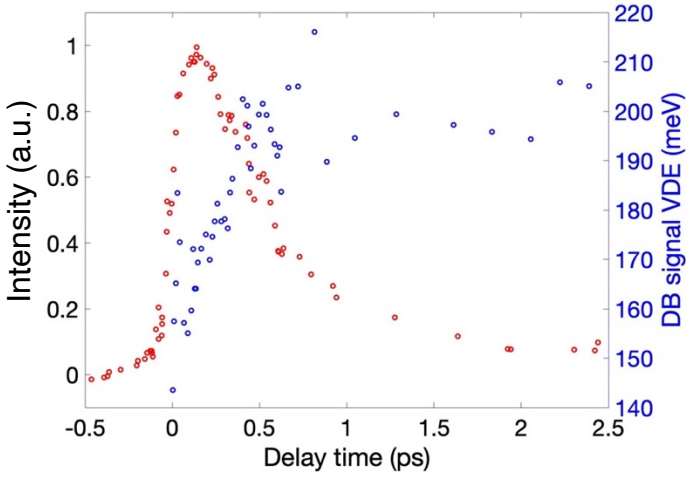

Figure 8. Vertical detachment energies and normalized signal intensity for Feature A (dipole-bound ion) up to 2.5 ps.

rapid decay of the DB state, these values can be extracted only for the first 1-2 picoseconds following excitation, but over this time frame the VDE of the DB state increases by about 50 meV, following a trend observed in the DB VDE values observed for I^-U and $I^-U{\cdot}H_2O$.[45, 51]

Figure 9 shows the integrated signal from feature D for both excitation energies probed at 3.14 eV. The rise of the feature is slow enough that the Gaussian term is unnecessary, and the data can be fit using a simple exponential rise and intensity offset, as in Eq 2.

$$I(t) = \begin{cases} 0, & t < 0 \\ I_{off} + A_i \exp\left(\frac{-t}{\tau_i}\right), & t \geq 0 \end{cases} \qquad \text{Eq. 2}$$

The rise time for I^- signal at each excitation energy is given in Table 3, as well as corresponding times measured for I-2thiouracil ($I^-{\cdot}2TU$). Higher energy excitation corresponds to a slightly faster dissociation, with 3.88 eV and 4.16 eV excitation resulting in rise times of 56 ps and 41 ps,

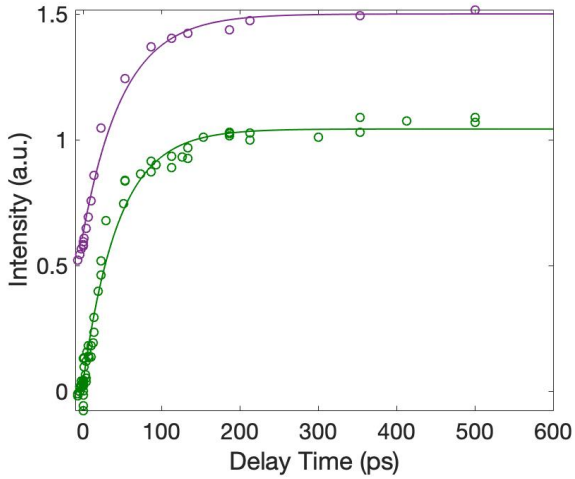

Figure 9. Time evolution of normalized, integrated Feature D for 4.16eV (green) or 3.88 eV (purple) excitation and 3.14 eV probe spectra. Plot at 3.88 eV is offset vertically by 0.5 a.u. to improve readability.

Table 3. Timescales describing rise time of feature D for different clusters and excitation energies

I^-·4TU		I^-·2TU	
hν (eV)	τ (ps)	hν (eV)	τ (ps)
3.88	56.2±9.4		
4.16	40.9±7.6	4.16	13.9±1.6
		4.74	9.0±1.2

respectively. For near-VDE excitation at 4.16 eV, the I^- rise time for I^-·4TU is a factor of ~3 longer than that of I^-·2TU (14 ps).

We have previously used Rice-Ramsperger-Kassel-Marcus (RRKM) theory[67, 68] to model the dissociation of I^-·N to I^-+N for various iodide nucleobase clusters, where N is the nucleobase.[46, 50, 51] The energy and vibrational frequencies of the I^-·4TU cluster were calculated at the MP2/aug-cc-pVDZ level, and the sum and density of states determined by the Beyer-Swinehart direct count algorithm with the Stein-Rabinovitch modification.[69, 70] As the transition state is loose, the reaction rate is determined variationally by modifying the N1–I distance to find the lowest calculated rate constant. With the low frequency in-plane rocking and out-of-plane twisting modes treated as hindered internal rotors, as described in greater detail elsewhere,[46, 52] we calculate dissociation time constants of 17.0 ps with 3.88 eV excitation and 11.5 ps with 4.16 eV excitation at the bond dissociation energy of 1.04 eV found using the level of theory given in Section II. The dependence of these values on small changes in the bond dissociation energy is discussed in Section V.

V. Discussion

The results obtained provide several interesting insights into the general set of thiouracils and previously measured iodide-nucleobase clusters.

VB formation by 3.88 eV excitation

Excitation at 3.88 eV corresponds to a localized ππ* transition of 4TU, but lies below the VDE of the I^-·4TU cluster of 4.18 eV as determined by our photoelectron spectrum. Spectra show no evidence for DB state formation, so such a state is not acting as a gateway to the observed VB anion state.

Previous iodide-nucleobase measurements have similarly resulted in spectra with VB signal but not DB signal, but these were all taken at excitation energies at 4.5-4.7 eV, well above the cluster VDE.[41, 45, 50] It was postulated, based primarily on computational results, that VB anions were formed by chromophore-localized $\pi\pi^*$ excitation followed by electron transfer from the halide to the hole in the chromophore π orbital, as shown in Eq. 3 with N as the nucleobase.[46]

$$I^- \cdot N(\pi^4\pi^{*0}) \xrightarrow{h\upsilon_{pump}} I^- \cdot N(\pi^3\pi^{*1}) \rightarrow I \cdot N(\pi^4\pi^{*1}) \qquad \text{Eq. 3}$$

However, due to the high energy excitation, indirect electron scattering mechanisms involving capture of a photodetached electron from the I^- into the π* orbital, leading to the same final state, could not be ruled out.

The experimental results here provide strong empirical evidence for the $\pi\pi^*$ excitation scheme in Eq. 3. The generation of a π orbital vacancy makes charge transfer to the thiobase energetically favorable even at excitation below the cluster VDE. Our results further indicate that this process is sufficiently rapid to account for IRF limited (sub 80 fs) VB signal rise not only in

this system but also in the previous above-VDE excitation energy measurements in which no DB signal was observed.

The rapid disappearance of this signal (τ_1=140 fs) is attributed to back electron transfer (BET) that results in reformation of iodide, as in previous studies of similar clusters (Eq 4a).[41, 46, 51, 52, 71] BET becomes less favorable if the iodine moves away from the valence-bound anion, a reasonable expectation given that the iodine/VB anion interaction potential will be quite different from the ground state I^-·4TU potential. Once the I atom moves away, autodetachment (AD, Eq. 4b) can become the primary decay mechanism.

$$I \cdot 4TU_{VB}^- \xrightarrow{BET} I^- \cdot 4TU \qquad \text{Eq. 4a}$$

$$I \cdot 4TU_{VB}^- \rightarrow I \cdots 4TU_{VB}^- \xrightarrow{AD} I + 4TU + e^- \qquad \text{Eq. 4b}$$

The slower time constant, τ_2=9 ps, is then attributed to this latter process.

VB and DB dynamics with 4.16 eV excitation

Excitation of the cluster at 4.16 eV, near the experimentally determined VDE, results in both DB and VB transient anion signal, as we have seen in previous iodide-nucleobase measurements.[41, 45, 47-50, 62] The presence of the DB anion of 4TU is notable, as photoelectron spectroscopy of $4TU^-$ [42] and photodepletion spectroscopy of I^-·4TU[55] did not detect this dipole-bound species.

The DB signal of I^-·4TU decays in 440 fs, whereas measurements of the I^-·2TU cluster show DB signal that arise and almost entirely decay within the instrument response time. This is a rather significant change in dynamics due to thionation position, with the conversion for I^-·2TU remaining anomalously rapid compared to I^-·U, I^-·4TU and I^-·U·H_2O. It suggests that geometric concerns or the nearly degenerate $\pi\pi^*$ excitations of neutral 2TU may play a role in its unusual

dynamics that bears further investigation.

The DB signal decays almost entirely within 2 ps, with a negligible signal offset at longer time delay. This result is similar to dynamics observed for $I^-\cdot 2TU$, and $I^-\cdot CH_3NO_2$, in which conversion from DB to VB is relatively complete. By comparison, DB signal from near-VDE excited $I^-\cdot U$ and $I^-U\cdot H_2O$ clusters exhibit bi-exponential decay, with a large portion of the signal remaining after several ps. The complete DB to VB conversion of the $I^-\cdot 4TU$, $I^-\cdot 2TU$, and $I^-\cdot CH_3NO_2$ clusters is consistent with a VB state lower in energy than the DB state.[35, 43, 72]

The VDE of the DB signal demonstrates a shift to higher binding energy over the first 1-2 ps following excitation (Fig 8). This shift has been attributed to motion of the neutral iodine, as increased distance between iodine and the DB anion reduces volume exclusion effects that destabilize the DB state at the shortest pump/probe delay times.[45, 51] Comparable measurements in $I^-\cdot U$ and $I^-\cdot U\cdot H_2O$ have shown that the VDE reaches an asymptote in 15–20 ps that agrees with that of the bare DB anion, suggesting that the iodine has fully dissociated from the cluster. Owing to the short-lived DB anion of $I^-\cdot 4TU$, we are unable to fully replicate this measurement. However, the VDE shifts in the first 1-2 ps suggest that initial iodine motion in $I^-\cdot 4TU$ is similar to the other clusters.

For VB signal formed by 4.16 eV excitation, an initial rise is seen within the experimental response time, followed by rapid decay (τ_1) and then a second signal rise (τ_2). The two distinct rise features indicate two VB formation mechanisms. The initial, IRF-limited rise can be attributed to the same mechanism underlying VB signal appearance with 3.88 eV excitation; the $\pi\pi^*$ excitation is accessible with a 4.1 6eV pump pulse, allowing for prompt transfer of the excess iodide electron to the π orbital vacancy. The second rise time τ_2 for the VB state can be fit well using the decay time for the DB state, indicating DB to VB conversion. The second rise τ_2 is absent for VB signal

under 3.88 eV excitation, given that no DB population is formed. With 4.16 eV excitation, however, we are able to see both VB formation mechanisms contributing to the overall signal level.

The VB signal offset observed at long time delays is consistent with the calculated stability of the VB state of $4TU^-$ and its measurement as a photoproduct of $I^-{\cdot}4TU$ in previous work.[43, 55] The VB signal generated at 4.16 eV retains most of its strength after 10 ps, in contrast to the VB signal from 3.88 eV excitation. This can be justified by considering the two VB formation mechanisms active at the higher excitation energy. The initial population of VB anions is depleted by rapid back electron transfer for both excitation energies, represented by decay constant τ_1. Only for near-VDE excitation does DB to VB formation contribute to VB signal strength after nearly 500 fs. As discussed above, the DB VDE shifts noticeably within this time frame, indicating that iodine has moved from its initial position in the anion ground state. This inhibits back electron transfer compared to the initial cluster geometry, with bond-lengthened clusters likelier to undergo AD. Moreover, AD is the only possible decay mechanism once the I atom fully leaves the cluster.

Autodetachment dynamics

Autodetachment (AD) of the excess electron is apparent in the one color spectra in Fig. 2 at both excitation energies. In previous time-resolved measurements of $I^-{\cdot}U$ and $I^-{\cdot}T$, the AD signal exhibits a distinct depletion around t_0, as the probe pulse detaches transients that would otherwise undergo AD.[48] In $I^-{\cdot}4TU$, as in $I^-{\cdot}U{\cdot}H2O$,[50] the depletion is not obvious, suggesting a VB state that is stabilized relative to AD.

Instead, the time-resolved spectra in Fig. 3–4 show significant enhancement of low eKE signal at positive time delays up to ~20ps, "overshooting" the baseline level established at negative time delays. This suggests that the 1.55 eV pulse is not purely acting as a probe pulse, but produces

a new state that can decay by AD. The autodetachment signal rise lags behind that of the VB by a few hundred femtoseconds, indicating that the new state may be an excitation of the VB anion, as shown in Eq 5.

$$\mathrm{I}\cdot 4\mathrm{TU}^{-}_{\mathrm{VB}} \xrightarrow{h\nu_{probe}} [\mathrm{I}\cdot 4\mathrm{TU}^{-}_{\mathrm{VB}}]^{*} \xrightarrow{AD} \mathrm{I}\cdot 4\mathrm{TU} \quad + e^{-} \qquad \text{Eq. 5}$$

The existence of a higher-lying VB excited state was previously postulated based on measurements of the $I^{-}\cdot U\cdot H_2O$[41, 50] and $I^{-}\cdot U$,[48] clusters which also show significant overshoot at positive time delays. However, $I^{-}\cdot T$, which exhibits rapid, nearly mono-exponential decay of the VB state, lacks this AD enhancement.[48] The strongest predictor of the AD overshoot seems to be VB anion signal that lasts longer than ~5 ps, further strengthening the assignment of feature C to AD from an excited VB state.

The AD signal enhancement decays with time constants of ~18 ps and ~16 ps for 3.88 eV and 4.16 eV excitation respectively. For $I^{-}\cdot U$ and $I^{-}U\cdot H_2O$, the intensity of the AD signal mirrors the decay of population of the VB state.[48, 50] This does not appear to be true for the $I^{-}\cdot 4TU$ cluster. In particular, a very large fraction of VB signal remains at 100ps in the case of 4.16 eV excitation due to the stability of the VB anion, whereas the AD signal enhancement decays entirely. This discrepancy may arise from dynamics in the cluster that impact the accessibility of the $4TU^{*}_{\mathrm{VB}}$ state but do not significantly alter the VB state itself, such as a change to solvation effects from neutral iodine motion.

Decay products

Photofragment product spectroscopy performed by Uleanya et al. indicate that $I^{-}\cdot 4TU$ clusters excited at 4 eV produce atomic I^{-} as a major photofragment and the deprotonated thiobase

$[4TU\text{-}H]^-$ as a very minor photofragment.[55] Dissociation of I^- is directly measured in our setup with the 3.14 eV probe pulse, which shows a signal rising mono-exponentially with time constants of 56 ps for the 3.88 eV pump energy and 41 ps for the 4.16 eV pump energy. Iodide may be reformed by back electron transfer (Eq. 4a), and the vibrationally excited cluster can then dissociate, as shown in Eq 6.

$$I \cdot 4TU_{VB}^- \xrightarrow{BET} I^- \cdot 4TU \rightarrow I^- + 4TU \qquad \text{Eq. 6}$$

As discussed in Section IV, the experimental dissociation times are nearly four times larger than those calculated by RRKM using the calculated bond dissociation energy of 1.04 eV. The calculated dissociation time of the I^-·2TU cluster, by contrast, is in good agreement with the experimental value.[52]

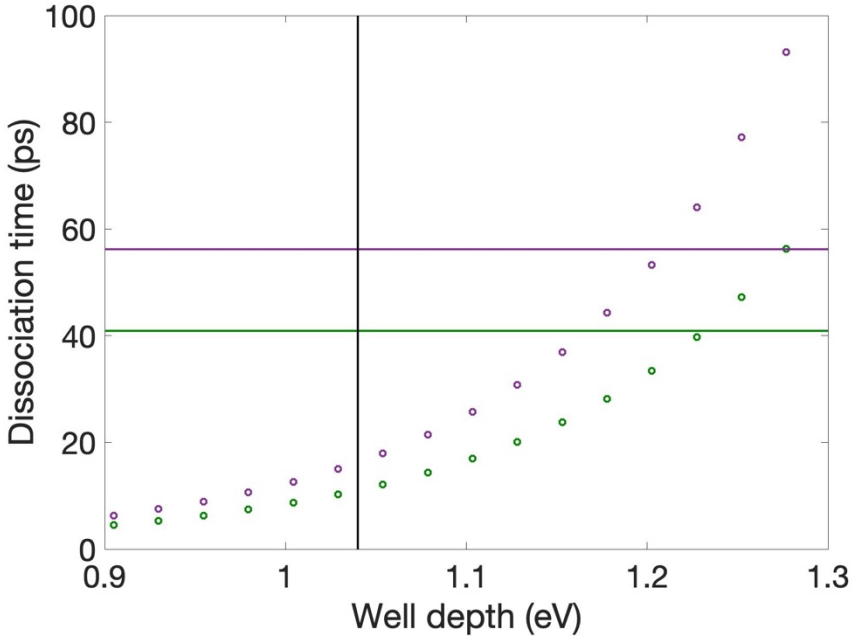

Figure 10. RRKM calculated dissociation time vs dissociation potential well depth for 3.88 eV (purple) and 4.16 eV(green) excitation. Experimental dissociation time constants are plotted as horizontal lines and the calculated depth given by the vertical line at 1.04 eV

While one might attribute this discrepancy to a mechanistic difference between I^-·4TU and I^-·2TU, the results of the RRKM calculation are highly dependent on the energy difference between the reactant and the calculated transition state. Fig 10 shows cluster dissociation time constants for I^-·4TU associated with different potential well depths with all other parameters equal. The well depth itself is a calculated value involving a loose, barrierless transition state, and therefore somewhat uncertain. Increasing the well depth by about 15% results in a calculated time constant that agrees with the experimentally determined I^- rise time. Alternatively, the well depth can be approximated from experimental values as the difference between the cluster VDE and the electron affinity of atomic I, or 4.18 eV - 3.06 eV = 1.12 eV. Even this correction would be sufficient to bring the RRKM calculation dissociation time within a factor of 2 of the experimental value. It is therefore likely that the discrepancy between calculated and experimental dissociation times in I^-·4TU is caused by uncertainty of the well depth, and that the same mechanism for I^- production, Eq. 6, holds for I^-·4TU and I^-·2TU.

VI. Conclusion

TRPES has been used to examine charge transfer dynamics of the I^-·4TU binary cluster. Excitation at 3.88 eV gives rise to VB signal without the mediation of a DB "gateway state". Rather, a localized $\pi\pi^*$ excitation of the chromophore allows for electron transfer to a vacancy in an energetically accessible π orbital of 4TU. The low energy $\pi\pi^*$ excitation of 4TU rules out other mechanistic possibilities, vindicating this pathway as a method of transient formation. Excitation at 4.16 eV leads to both VB and DB signal, with the transition between DB and VB states clear in the spectra taken with 1.55 eV probe.

At both excitation energies, the VB state decays by rapid back-electron transfer to the I

atom and a slower process attributed to autodetachment. In addition, at positive pump-probe delays we observe enhanced slow photoelectron signal attributed to probe-pulse excitation (1.55 eV) of the VB state to a higher-lying state that undergoes autodetachment. Finally, with the 3.14 eV probe pulse, we find that dissociation to I^-+4TU occurs on a time scale of 10s of ps. This channel is attributed to back-electron transfer to form vibrationally excited I^-·4TU followed by statistical ground state dissociation.

This work shows that there are distinct differences in the dynamics of photoexcited I^-·4TU compared to I^-·2TU and iodide complexes with the canonical nucleobases. The most important of these arises owing to the presence of a ππ* transition below the cluster VDE in I^-·4TU. It will be of considerable interest to see if the dynamics of iodide complexed with 2,4-dithiouracil (I^-·2,4TU) lie closer to those of I^-·4TU or I^-·2TU; these studies are currently underway in our laboratory.

Acknowledgments

This research was supported by the National Science Foundation under Grant No. CHE-2154629 and by CALSOLV, the Center for Solvation Studies at the University of California, Berkeley. MK thanks the support of the Japan Society for the Promotion of Science (JSPS) Overseas Research Fellowships.

References

1. S. Matsika, J. Phys. Chem. A **108**, 7584–7590 (2004).
2. C. E. Crespo-Hernández, B. Cohen, P. M. Hare and B. Kohler, Chem. Rev. **104**, 1977–2020 (2004).
3. A. Stolow, A. E. Bragg and D. M. Neumark, Chem. Rev. **104** (4), 1719–1758 (2004).
4. C. T. Middleton, K. de La Harpe, C. Su, Y. K. Law, C. E. Crespo-Hernández and B. Kohler, Annu. Rev. Phys. Chem. **60**, 217–239 (2009).
5. M. Barbatti, A. J. A. Aquino, J. J. Szymczak and H. Lischka, Proc. Natl. Acad. Sci. U.S.A. **107** (50), 21453–21458 (2010).
6. R. Improta, F. Santoro and L. Blancafor, Chem. Rev. **116** (6), 3540–3593 (2016).
7. H. Yu, J. A. Sánchez-Rodríguez, M. Pollum, E. Crespo-Hernandez, S. Mai, P. Marquetand, L. Gonzalez and S. Ullrich, Phys. Chem. Chem. Phys. **18**, 20168–20176 (2016).
8. L. Martínez-Fernández, G. Granucci, M. Pollum, C. E. Crespo-Hernandez, M. Persico and I. Corral, Chem. Eur. J. **23** (11), 2478–2728 (2016).
9. M. Pollum, S. Jockusch and C. E. Crespo-Hernandez, J. Am. Chem. Soc. **136**, 17930–17933 (2014).
10. M. Pollum and C. E. Crespo-Hernández, J. Chem. Phys. **140**, 071101 (2014).
11. M. Pollum, S. Jockusch and C. E. Crespo-Hernandez, Phys. Chem. Chem. Phys. **17**, 27851–27861 (2015).
12. S. Mai, P. Marquetand and L. González, J. Phys. Chem. Lett. **7** (11), 1978–1983 (2016).
13. S. Mai, M. Pollum, L. Martínez-Fernández, N. Dunn, P. Marquetand, I. Corral, C. E. Crespo-Hernández and L. González, Nat. Commun. **7**, 13077 (2016).
14. J. A. Sánchez-Rodríguez, A. Mohamadzada, S. Mai, B. Ashwood, M. Pollum, P. Marquetand, L. González, C. E. Crespo-Hernández and S. Ullrich, Phys. Chem. Chem. Phys. **19** (30), 19756–19766 (2017).
15. A. Mohamadzade, S. Bai, M. Barbatti and S. Ullrich, Chem. Phys. **515**, 572–579 (2018).
16. S. Ullrich, Y. Qu, A. Mohamadzade and S. Shrestha, J. Phys. Chem. A **126** (44), 8211–8217 (2022).
17. A. Mohamadzade, A. Nenov, M. Garavelli, I. Conti and S. Ullrich, J. Am. Chem. Soc. **145**, 11945–11958 (2023).
18. L. A. Ortiz-Rodrìguez and C. E. Crespo-Hernàndez, Chem. Sci. **11**, 11113–11123 (2020).
19. V.-H. Nguyen, S. Heo, C. W. Koh, J. Ha, G. Kim, S. Park and Y. Yoon, ACS Sens. **6** (9), 3462–2467 (2021).
20. B. Boudaïffa, P. Cloutier, D. Hunting, M. A. Huels and L. Sanche, Science **287**, 1658–1660 (1998).
21. J. Narayanan S J, D. Tripathi, P. Verma, A. Adhikary and A. K. Dutta, ACS Omega **8** (12), 10669-10689 (2023).
22. M. S. Robinson, M. Niebuhr and M. Gühr, Molecules **28**, 2354 (2023).
23. R. Barrios, P. Skurski and J. Simons, J. Phys. Chem. B **106**, 7991–7994 (2002).
24. J. Berdys, I. Anuseiwicz, P. Skurski and J. Simons, J. Am. Chem. Soc **126**, 6441º6447 (2004).
25. F. Martin, P. D. Burrow, Z. L. Cai, P. Cloutier, D. Hunting and L. Sanche, Phys. Rev. Lett. **93**, 068101 (2004).
26. J. Simons, Acc. Chem. Res. **39**, 772–779 (2006).
27. G. Hanel, B. Gstir, S. Denifl, P. Scheier, M. Probst, B. Farizon, M. Farizon, E. Illenberger

and T. D. Märk, Phys. Rev. Lett. **90** (18) (2003).
28. S. Denifl, S. Ptasinska, M. Cingel, S. Matejcik, P. Scheier and T. D. Märk, Chem. Phys. Lett. **377**, 74–80 (2003).
29. H. Abdoul-Carime, M. A. Huels and E. Illenberger, Eur. Phys. J. D **35**, 399–404 (2005).
30. P. Burrow, G. A. Gallup, A. M. Scheer, S. Denifl, S. Ptasinska, T. Mark and P. Scheier, J. Chem. Phys. **125** (12), 124310 (2006).
31. D. Huber, M. Beikircher, S. Denifl, F. Zappa, S. Matejcik, A. Bacher, V. Grill and T. D. Märk, J. Chem. Phys. **125**, 084304 (2006).
32. J. Kopyra, H. Abdoul-Carime, F. Kossoski and M. d. N. Varella, Phys. Chem. Chem. Phys. **16** (45), 25054–25061 (2014).
33. J. Kopyra and H. Abdoul-Carime, J. Chem. Phys. **144**, 034306 (2016).
34. J. Kopyra, K. K. Kopyra, H. Abdoul-Carime and D. Branowska, J. Chem. Phys. **148** (23), 234301 (2018).
35. J. H. Hendricks, S. A. Lyapustina, H. L. d. Clercq, J. T. Snodgrass and K. H. Bowen, The Journal of Chemical Physics **104** (19), 7788-7791 (1996).
36. X. Li, K. H. Bowen, M. Haranczyk, R. A. Bachorz, K. Mazurkiewicz, J. Rak and M. Gutowski, J. Chem. Phys. **127** (17), 174309 (2007).
37. J. Schiedt, R. Weinkauf, D. M. Neumark and E. W. Schlag, Chem. Phys. **239**, 511–524 (1998).
38. J. Simons, J. Phys. Chem. A **112** (29), 6401–6511 (2008).
39. O. H. Crawford, Mol. Phys. **20** (4), 585–591 (1971).
40. R. A. Bachorz, W. Klopper, M. Gutowski, X. Li and K. H. Bowen, J. Chem. Phys. **129** (5), 054309 (2008).
41. A. Kunin and D. M. Neumark, Phys. Chem. Chem. Phys. **21** (14), 7239–7255 (2019).
42. X. Li, J. Chen and K. H. Bowen, J. Chem. Phys. **134** (7), 074304 (2011).
43. O. Dolgounitcheva, V. Zakrzewski and J. Ortiz, J. Chem. Phys. **134** (7), 074305 (2011).
44. E. Matthews, R. Cercola, G. Mensa-Bonsu, D. M. Neumark and C. E. Dessent, J. Chem. Phys. **148** (8), 084304 (2018).
45. S. B. King, M. A. Yandell, A. B. Stephansen and D. M. Neumark, J. Chem. Phys. **141** (22), 224310 (2014).
46. W.-L. Li, A. Kunin, E. Matthews, N. Yoshikawa, C. E. Dessent and D. M. Nuemark, J. Chem. Phys. **145** (4), 044319 (2016).
47. M. A. Yandell, S. B. King and D. M. Neumark, J. Am. Chem. Soc. **135** (6), 2128–2131 (2013).
48. S. B. King, M. A. Yandell and D. M. Neumark, Faraday Discuss. **163**, 59–72 (2013).
49. A. B. Stephansen, S. B. King, Y. Yokoi, Y. Minoshima, W.-L. Li, K. A., T. Takayanagi and D. N. Neumark, J. Chem. Phys. **143** (10), 104308 (2015).
50. A. Kunin, V. S. McGraw, K. G. Lunny and D. M. Neumark, J. Chem. Phys. **151** (15), 154304 (2019).
51. A. L. Kunin, W.-L.; Neumark, D. M., J. Chem. Phys. **149** (8), 084301 (2018).
52. M. Koga, M. Asplund and D. M. Neumark, J. Chem. Phys. **156**, 24302 (2022).
53. R. Cercola, E. Matthews and C. E. H. Dessent, Mol. Phys. **21**, 3001–3010 (2019).
54. K. O. Uleanya, R. Cercola, M. Nikolova, E. Matthews, N. G. K. Wong and C. E. Dessent, Molecules **25** (14), 3157 (2020).
55. K. O. Uleanya and C. E. Dessent, Phys. Chem. Chem. Phys. **23** (2), 1021–1030 (2021).
56. A. V. Davis, R. Wester, A. E. Bragg and D. M. Neumark, The Journal of Chemical Physics

118 (3), 999-1002 (2003).
57. A. E. Bragg, J. R. R. Verlet, A. Kammrath, O. Cheshnovsky and D. M. Neumark, Journal of the American Chemical Society **127** (43), 15283-15295 (2005).
58. W. Wiley and I. H. McLaren, Rev. Sci. Instrum. **26** (12), 1150–1157 (1955).
59. V. Dribinski, A. Ossadtchi, V. A. Mandelshtam and H. Reisler, Rev. Sci. Instrum. **73** (7), 2634–2642 (2002).
60. M. J. Frisch, G. W. Trucks, H. B. Schlegel, G. E. Scuseria, M. A. Robb, J. R. Cheeseman, G. Scalmani, V. Barone, G. A. Petersson, H. Nakatsuji, X. Li, M. Caricato, A. V. Marenich, J. Bloino, B. G. Janesko, R. Gomperts, B. Mennucci, H. P. Hratchian, J. V. Ortiz, A. F. Izmaylov, J. L. Sonnenberg, D. Williams-Young, F. Ding, F. Lipparini, F. Egidi, J. Goings, B. Peng, A. Petrone, T. Henderson, D. Ranasinghe, V. G. Zakrzewski, J. Gao, N. Rega, G. Zheng, W. Liang, M. Hada, M. Ehara, K. Toyota, R. Fukuda, J. Hasegawa, M. Ishida, T. Nakajima, Y. Honda, O. Kitao, H. Nakai, T. Vreven, K. Throssell, J. Montgomery, J. A., J. E. Peralta, F. Ogliaro, M. J. Bearpark, J. J. Heyd, E. N. Brothers, K. N. Kudin, V. N. Staroverov, T. A. Keith, R. Kobayashi, J. Normand, K. Raghavachari, A. P. Rendell, J. C. Burant, S. S. Iyengar, J. Tomasi, M. Cossi, J. M. Millam, M. Klene, C. Adamo, R. Cammi, J. W. Ochterski, R. L. Martin, K. Morokuma, O. Farkas, J. B. Foresman and D. J. Fox, *Gaussian 16, Rev. A.03*. (Gaussian, Inc.: Wallingford, CT, 2016).
61. K. A. Peterson, B. C. Shepler, D. Figgen and H. Stoll, J. Phys. Chem. A **110** (51), 13877–13883 (2006).
62. S. B. King, A. B. Stephansen, Y. Yokoi, M. A. Yandell, A. Kunin, Y. Takayanagi and D. M. Neumark, J. Chem. Phys. **143** (2), 024312 (2015).
63. R. J. Peláez, C. Blondel, C. Delsart and C. Drag, J. Phys. B: At. Mol. Opt. Phys. **42**, 125001 (2009).
64. A. Kunin, W.-L. Li and D. M. Neumark, J. Chem. Phys. **149** (8), 084301 (2018).
65. Sommerfeld, J. Phys. Chem. A. **108** (42), 9150–9154 (2004).
66. J. Narayanan S J, D. Tripathi and A. K. Dutta, J. Phys. Chem. Lett. **12** (42), 10380–10387 (2021).
67. T. Baer, W. L. Hase and L. William, *Unimolecular reaction dynamics: theory and experiments*. (Oxford University Press on Demand, 1996).
68. R. G. Gilbert and S. C. Smith, *Theory of unimolecular and recomination reactions*. (Publishers' Business Services, 1990).
69. T. Beyer and D. Swinehard, Communications of the ACM **16** (6), 379 (1973).
70. S. E. Stein and B. Rabinovitch, J. Chem. Phys. **58** (6), 2438–2445 (1973).
71. A. Kunin, W.-L. Li and D. M. Neumark, Phys. Chem. Chem. Phys. **18**, 33226 (2016).
72. R. A. Bachorz, W. Klopper and M. Gutowski, The Journal of Chemical Physics **126** (8), 085101 (2007).